The final publication is available at

https://doi.org/10.1109/JLT.2021.3115084

Additional Information

Remote Photonic THz Generation using an Optical Frequency Comb and Multicore Fiber

Maria Morant, *Member, IEEE,* Luis Gonzalez-Guerrero, *Member, IEEE,*
Cyril C. Renaud, *Member, IEEE* and Roberto Llorente, *Member, IEEE*

Abstract— This paper proposes and demonstrates a photonic THz generation technique based on an optical frequency comb and multicore fiber (MCF) transmission, with the advantage of remote generation with great reconfigurability and reduced digital signal processing (DSP). The feasibility of the proposed technique is evaluated experimentally comparing the performance when transmitting a data wavelength and a local oscillator for optical heterodyning over a single core or over different cores in a 1-km MCF link. The proposed remote photonic THz generation technique is demonstrated employing a 16QAM 12.5 GBd signal. A short wireless transmission at 183 GHz center frequency with 0.25 m antenna-separation is achieved after 1 km MCF, meeting the soft-decision decision forward error correction (SD-FEC) bit error rate (BER) recommendation of $2 \cdot 10^{-2}$. The analysis includes the received photocurrent range for which the BER meets the standard hard-decision forward error correction (HD-FEC) recommendation of $3.8 \cdot 10^{-3}$ BER. The BER performance is analyzed considering different DSP configurations, with and without frequency offset estimation (FOE) and decision-driven least mean squares (DD LMS) equalization. The performance of the remote photonic THz generation technique is evaluated comparatively against traditional free-running laser transmission over MCF, confirming the advantage of using comb generation to reduce the frequency offset fluctuation and simplify the DSP.

Index Terms— Microwave photonics, millimeter wave communication, optical mixing, optical frequency comb generator, digital signal processing (DSP), multicore fiber (MCF)

I. INTRODUCTION

HIGH-SPEED wireless communications at Terahertz (THz) frequencies (from 100 GHz to 10 THz) have been proposed as a suitable technology for ultrahigh data rate applications to overcome the spectrum scarcity at lower RF frequencies [1]. The large bandwidth (BW) available in the THz spectrum (i.e. several tens of GHz), compared to millimeter-wave systems, permits the use of simpler and lower-order modulation formats, thus reducing the system complexity and the transceivers power consumption. However, considering the limited wireless reach in THz communications due to free-space transmission losses, the optical distribution of THz signals and further wireless generation is indicated as a straight-forward solution to achieve THz coverage in wide range areas

[2]. Seamless integration of broadband wireless and optical networks is possible thanks to the rapid deployment of optical access networks and the growing availability of mature and cost-effective opto-electronic technologies [3]. In the last decades, radio-over-fiber techniques have been studied extensively as a cost- and power-efficient solution for the optical-wireless network integration simplifying both the base-stations and remote nodes [3]. This approach can be further extended to multi-carrier support, maximizing the overall channel data rate and increasing the spectral efficiency [4].

The most promising photonic technique for broadband THz generation is based on the heterodyning of two different wavelengths which are mixed at the receiver photodiode (also commonly referred as photomixer), producing an electrical signal whose frequency is the difference between both wavelengths [2]. The photomixer is a key component of THz wireless-over-fiber systems where unitraveling-carrier photodiodes (UTC-PDs) provide a combination of high optical responsivity, large BW and high THz output power [2], achieving over 300 GHz BW and RF output power higher than 20 mW at 100 GHz [5]. Coherent optics provides a higher receiver sensitivity and enables the compensation of linear transmission impairments such as chromatic dispersion and polarization mode dispersion [6]. In the target application scenario, digital signal processing (DSP), coherent detection with Schottky barrier diode (SBD)-based mixers and spectrally-efficient advanced modulations enabled the implementation of digital coherent THz systems [7]. Using free-running lasers requires heavy carrier recovery and carrier phase noise correction processes in the DSP, increasing the processing time, complexity and power consumption [4]. To generate the different carriers, an optical frequency comb generator (OFCG) is proposed to be used to obtain phase-correlated optical signals. Recently, full-duplex transmission providing data-rates up to 256 Gbit/s has been demonstrated using an OFCG over 80 km of single-mode fiber (SMF) [6]. In this work, we go a step further with the combination of OFCG and multicore fiber (MCF), with the advantage of remote generation and reconfigurability as depicted in Fig. 1.

M. Morant and R. Llorente are with the Nanophotonics Technology Center, Universitat Politècnica de València, 46022 Valencia, Spain (e-mail: mmorant@ntc.upv.es; rllorent@ntc.upv.es).

L. Gonzalez-Guerrero is with Grupo de Optoelectrónica y Tecnología Laser (GOTL) of Departamento de Tecnología Electrónica, Universidad Carlos III de Madrid, Madrid 28911, Spain (e-mail: lgguerre@ing.uc3m.es).

C. C. Renaud is with the Department of Electronic and Electrical Engineering, University College London, London WC1E 7JE, U.K. (e-mail: c.renaud@ucl.ac.uk).
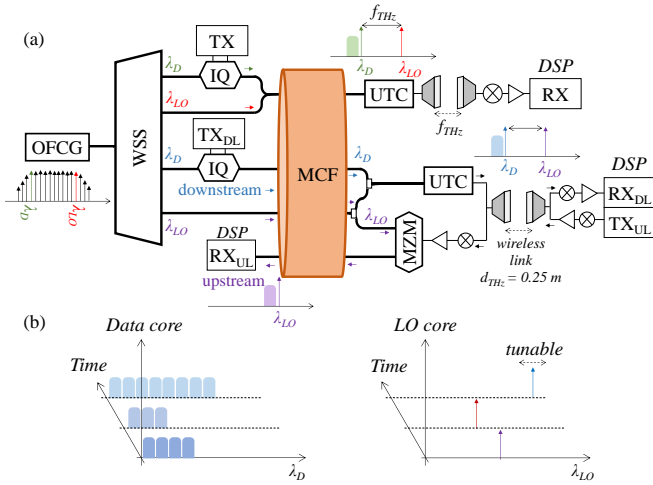
Fig. 1. (a) Block diagram of photonic THz generation using OFCG and MCF using the same or different cores for LO transmission. TX: transmitter, RX: receiver, WSS: wavelength selective switch, IQ: I/Q modulator, MZM: Mach-Zehnder modulator. UTC: Unitraveling-carrier photodiode. (b) Scheme of wavelength distribution when the data and LO carriers are transmitted over different cores of the MCF.

MCF comprising several cores in a single fiber improves the SMF transmission capacity by using spatial division multiplexing (SDM) over the different cores of the same media with improved efficiency in limited-space scenarios [8]. MCF has been indicated for elastic optical networks by using a flexible spectrum grid and DSP for inter-core crosstalk suppression [9] and we recently demonstrated its suitability for integrated wireless-optical backhaul and fronthaul provision [10]. In this work, as depicted in Fig. 1, the comb lines are split so one line is optically modulated with data (λ_D) and another line is used as optical local oscillator (λ_{LO}) for optical heterodyning at the photomixer, obtaining a RF wireless transmission at 183 GHz center frequency (window of atmosphere water vapor absorption, also referred as sub-THz or THz frequency). The directionality provided in short-wireless communications in the THz band increases the isolation with reduced interference, which is suitable for rack-to-rack interconnection in data centers [11] and other high data-rate applications. We compare the experimental performance of transmitting both wavelengths over the same or over different cores of a MCF link using different DSP configurations. Since the 1990s, digital coherent receivers have demonstrated to provide improved sensitivity while allowing to overcome optical impairments –such as chromatic dispersion or polarization mode dispersion (PMD)– which enabled the deployment of high-speed systems [7].

Digital coherent receivers also enabled new network architectures due to its more robust transmission and rerouting capabilities [7]. As depicted in Fig. 1(b), transmitting the optically modulated data signal and the optical LO signal over different cores provides more adaptability to the system, as it enables using the same LO for different purposes (i.e. THz generation of other data wavelengths or optical modulation for upstream signals allowing a frequency reuse system as depicted in Fig. 1(a)). In addition, it provides more flexibility in the spectrum usage as the LO carrier can be tuned depending on the desired frequency band and on the number of data channels to

be transmitted, as depicted in Fig. 1(b).

This paper is structured as follows: Section II describes the laboratory system deployed for the experimental evaluation of both photonic THz generation techniques employing OFCG and MCF, and the coherent DSP routine implemented at the receiver, which is later evaluated with different configurations. Next, in section III, the bit error rate (BER) performance after 1 km of MCF transmission is compared in terms of the received optical power and photocurrent level. In the experimental analysis, different DSP configurations are evaluated taking into account the number of taps employed for the equalization. In addition, the wavelength stability of the optical LO generated with the OFCG is evaluated and compared with conventional free-running laser generation over the same arrangement. Section III also includes the discussion for extending the wireless reach and a simulation study regarding the optical signal to noise ratio (OSNR) required at the receiver for extending the optical reach. Finally, in Section IV, the main conclusions of this work are highlighted.

II. SYSTEM DESCRIPTION

A. Optical frequency comb generator (OFCG)

Fig. 2(a) shows the block diagram of the OFCG consisting of a tunable external cavity laser (ECL) operating at λ_{ECL}=1553.33 nm and a LiNbO$_3$ dual-drive Mach-Zehnder modulator (DD-MZM), which is an effective method for generating phase correlated optical tones equally spaced by the driving RF-frequency [11]. The modulator is dual-driven with sinusoidal signals generated from a synthesizer (LO) and divided in two branches with a hybrid coupler. The phase difference between RF-a and RF-b is aligned to zero with a phase shifter (PS) placed in the feeder cable for RF-a [12]. The intensity of RF-a is also attenuated (Att) compared with RF-b to obtain a spectrally-flat optical comb [13]. Several comb configurations were tested experimentally as shown in Fig. 2(b) and (c) with different line separation. Two optical lines of the comb can be selected by using narrow optical filters or with optical laser locking techniques. In this case, we used a wave-shaper (WSS Finisar 4000S) as depicted in Fig. 5.
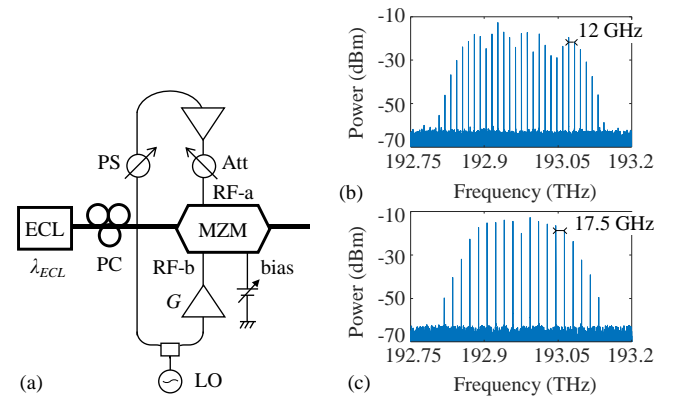

Fig. 2. (a) Block diagram of the OFCG and resulting optical spectra (RBW = 10 MHz) with line separation (LO RF configuration) of: (b) 12 GHz and (c) 17.5 GHz
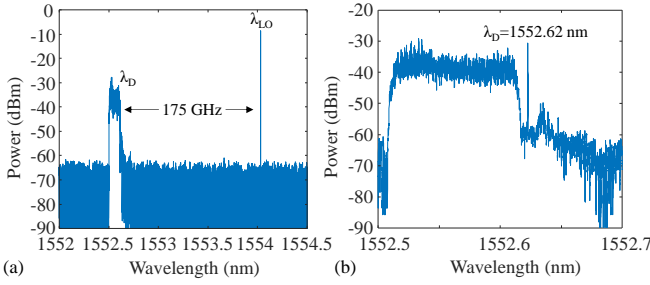
Fig. 3. Received optical spectra showing: (a) selected carriers for data signal modulation (λ_D) and optical LO signal (λ_{LO}) for photonic THz generation at f_{THz}=175 GHz obtained with OFCG with 17.5 GHz line separation and (b) zoom of the optically modulated data signal (λ_D)
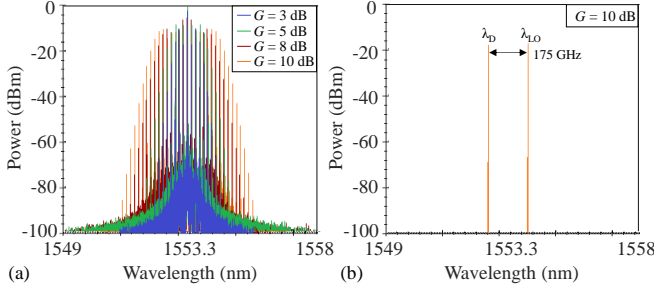

Fig. 4. Simulated optical spectra for different OFCG configurations using λ_{ECL}=1553.33 nm considering: (a) different electrical amplifier gains, and (b) filtered selected lines separated f_{THz}=175 GHz

For the experimental demonstration, the LO of the OFCG in Fig. 2(a) was set to 17.5 GHz (separation between optical lines), obtaining a separation between 10 carriers of f_{THz}=175 GHz with λ_D=1552.62 nm and λ_{LO}=1554.03 nm, as represented in the spectra shown in Fig. 3(a), measured after 1-km 7-core MCF transmission –commercially available Fibercore SM-7C1500(6.1/125)–.

The OFCG implementation in the experimental work is capable of generating 11 optical comb lines around a center frequency with a spectral ripple lower than 1.1 dB as reported in [12]. Recently, OFCG generation with 22 lines has been demonstrated covering 360 GHz BW span [11]. The OFCG is here configured to minimize the power difference between the two selected lines (centered at λ_D=1552.62 nm and λ_{LO}=1554.03 nm respectively). Further simulation study is performed with Optiwave design software (OptiSystem 18) considering the system diagram depicted in Fig. 2(a) in order to evaluate the comb spectrum. Fig. 4(a) shows the resulting spectra obtained for an electrical amplifier gains of G = 3, 5, 8 and 10 dB. It can be observed that the resulting number of comb lines and amplitude ripple can be tuned adjusting the gain G. Fig. 4(b) shows the simulation results obtained with G=10 dB, filtering two carriers separated 175 GHz (10 lines) at λ_D=1552.62 nm and λ_{LO}=1554.03 nm. It is confirmed that the resulting power difference between these two lines is smaller than 1 dB, as in the experimental spectra reported in Fig. 2(c).

B. Experimental setup

Fig. 5(a) emulates the conventional photonic THz generation technique where both the optically modulated data signal (λ_D) and the optical LO signal (λ_{LO}) are transmitted over the same core of the MCF (conventional would be over SMF).
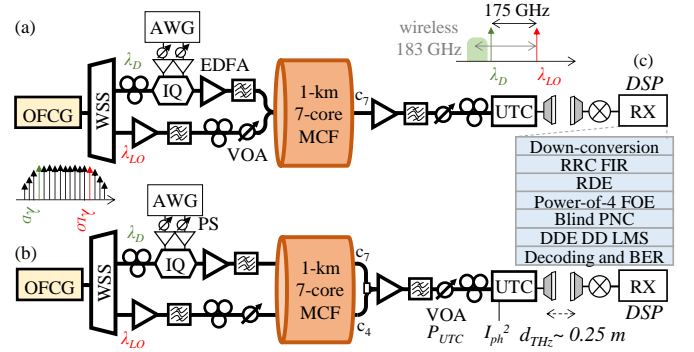

Fig. 5. Photonic THz generation experimental systems using an OFCG and MCF when optically modulated data signal (λ_D) and the optical LO signal (λ_{LO}) are transmitted over: (a) the same core and (b) different cores. (c) Steps implemented in the coherent DSP algorithm and main parameters

Fig. 5(b) shows the novel generation technique where λ_D and λ_{LO} are transmitted over different cores and combined after MCF transmission before the UTC for optical heterodyning.

The performance is evaluated experimentally with a 16-quadrature amplitude modulation (QAM) 12.5 GBd signal, which is transmitted wirelessly at 183 GHz, emulating an optical backhaul system. The in-phase and quadrature (I/Q) components of the analog 16-QAM signal are generated with an arbitrary waveform generator (AWG Tektronix 70001A) operating at 50 GSa/s. The digital I/Q signals are defined with Matlab® with four 2^{11} de Bruijn bit sequences mapped into 16-QAM with a symbol rate R_{symb}=12.5 GBd, filtered with root raised cosine (RRC) filters with passband bandwidth of 13.75 GHz (i.e., α = 0.1). The complex signal is upconverted to intermediate frequency (IF) of $f_{IF} = 0.6 \cdot R_{symb} = 7.5$ GHz and filtered for single sideband (SSB) signal transmission. The resulting electrical signals are time-aligned with two phase-shifters (PS) and electronically amplified (23 dB gain) before I/Q optical modulation. The modulated signal is amplified with an Erbium doped fiber amplifier (EDFA) and filtered. Depending on the arrangement of the MCF, the modulated data and the LO carriers are combined to be transmitted into the same core –core c7 as depicted in Fig. 5(a)– or are transmitted through different cores –cores c7 and c4, respectively– as indicated in Fig. 5(b).

A variable optical attenuator (VOA) is used to ensure that when mixed both λ_D and λ_{LO} are combined with -0.7 dBm optical power level each. After 1-km of MCF transmission the signal is amplified with an EDFA, filtered and a VOA is included before the UTC to test the performance with the received optical power level (maximum P_{UTC} < 16.5 dBm). Fig. 3(b) shows the optical spectra of the SSB modulated data over λ_D=1552.62 nm with the IQ modulation after 1-km of 7-core MCF transmission.

For THz generation, an unpackaged UTC-PD biased with -2 V is used as optical receiver. The received bit error rate (BER) is evaluated against the UTC photocurrent squared (I_{ph}^2) because it is proportional to the emitted THz power [14]. A wireless communication link is included in the system with horn antennas (20 dBi gain) separated d_{THz} = 0.25 m. In order to increase the collimation of the sub-THz beam at 183 GHz RF

center frequency, two Teflon lenses with 5-cm diameter and 75-mm back focal length are included between the horn antennas with 0.1 m separation. A short wireless distance is evaluated in order to be able to reduce the optical power arriving to the receiver, which limits the output power from the UTC-PD (estimated to be few µW). After wireless transmission, the received wireless signal is down-converted to intermediate frequency (IF) with a second-harmonic mixer (Virginia Diodes WR5.1SHM), electronically amplified (40 dB gain) and sampled with a high-bandwidth oscilloscope (LeCroy LabMaster 10-36Zi) operating at 80 GSa/s.

C. Coherent DSP algorithm

At the receiver, a coherent DSP routine is used as depicted in Fig. 5(c). A digital coherent receiver includes two main subsystems: the inner and outer receiver [11]. The inner receiver main functionality is to produce a "synchronized channel" as similar as possible to the theoretic communication. The outer receiver main functionality is to optimally decode the demodulated signals in order to produce the best estimate of the sequence of received bits [11]. The main steps of the coherent DSP routine implemented with Matlab® include:

1) Complex down-conversion considering f_{up} as IF.

2) RRC matched filtering with a roll-off factor $\alpha = 0.1$ and a filter span of 60 symbols.

3) Radius directed equalization (RDE) with order 18 and step vector = [0.01 0.001 0.0001]. The RDE optimization is based on the equalizer output and the nearest constellation radius [16]. The radius decision (R_k) is set to $R_k = 0.2$ for inputs $< (\sqrt{2}+1)/2$, $R_k = 1.8$ for inputs $> (1+\sqrt{1.8})/2$, and $R_k = 1$ for the rest.

4) Power-of-4 frequency offset estimation (FOE) using Fast Fourier Transform (FFT) calculation as $y_{FFT} = fft(y_n^4)$ where y_n is the normalized input [17]. Shifting the zero-frequency component to center of spectrum, we measure the frequency offset between the real IF and the estimated f_{up} in the first step of complex down-conversion.

5) Blind phase noise compensation (PNC) with a delta angle of $\pi/64$ [18].

6) Decision directed equalization (DDE) with decision-driven least mean squares (DD LMS). The order of the DD LMS equalization ($order = taps - 1$) is used to equalize the signal in blocks of $taps - 1$ number of samples. In order to obtain which is the optimum number of taps, this value is reduced (in steps of 2) until a bit error rate of BER $< 2 \cdot 10^{-2}$ is reached (corresponding to a 20%-overhead soft-decision SD-FEC). In this evaluation, we compare the performance of the DSP algorithm using a fixed number of taps (from 41 to 91 taps) with using the minimum number of taps.

7) Differential decoding is applied only to the first two bits in order to remove the quadrant ambiguity associated with square QAM constellations. For the rest pair of bits, no differential decoding is implemented. Then, the de Bruijin symbol sequence is retrieved. Cross correlation is performed to align the received bits comparing the received sequence with the original sequence and, then, compute the number of bit errors and BER. We analyze $2.5 \cdot 10^5$ bits per

point so, considering reliable estimates when at least 100 errors occur, the lowest reliable BER is around $4 \cdot 10^{-4}$. A target BER of $3.8 \cdot 10^{-3}$ corresponding to 7% redundancy hard-decision forward error correction (HD-FEC) [19] is considered, in addition to the previously-mentioned SD-FEC threshold.

III. EXPERIMENTAL RESULTS AND DISCUSSION

Fig. 6(a) shows the BER performance comparison when transmitting the comb data and the LO wavelengths over the same core of a 1-km MCF link –measured using the experimental setup depicted in Fig. 5(a)–, considering the central frequency measured at $f_{up} = 12.0989$ GHz. As reference, dashed lines are included in the BER graphs at $2 \cdot 10^{-2}$ for SD-FEC and $3.8 \cdot 10^{-3}$ for HD-FEC [19]. The concrete number of taps used in the DD LMS equalization (ranging from 41 to 91) are reported in Fig. 6(b). Fig. 7 shows the BER performance when the data and optical LO wavelengths are transmitted over different cores of the MCF –as depicted in Fig. 5(b)–. It can be observed that in both implementations (transmission of the optical LO over the same and different cores), for received photocurrent levels higher than 12 mA^2, saturation due to thermal or space-charge effects [20] start to be noticed in the BER performance in both Fig. 6(a) and Fig. 7(a).

In Fig. 6(a) and Fig. 7(a), no significant BER improvement is observed when increasing from 41 to 61 taps in the DD LMS equalization. This means that at least 64 samples (65 taps – 1) are needed in the DD LMS equalization process. In both transmission cases over the same and different cores, the minimum recommended number of taps for DD LMS equalization is 71 in order to increase the photocurrent range for which the HD-FEC BER is met. The range of received photocurrent is represented with bars in Fig. 8 for different number of taps compared with not implementing DD LMS equalization, also including the corresponding received optical power (P_{UTC}). The experimental results indicate that when both signals are transmitted in the same core, the range changes from [4.72 mA^2, 30.1 mA^2] with no DD LMS to [0.94 mA^2, 37.8 mA^2] when 71 taps or more are used in the DD LMS equalization. When the optical LO is transmitted in a different core, the received optical power and photocurrent range is smaller compared with the transmission over the same core performance, but it is only reduced in the upper values due to saturation effects. In particular, when transmitting over different cores, the received photocurrent meets the HD-FEC BER recommendation in the range from [6.12 mA^2, 19.75 mA^2] when no DD LMS is in place and to [0.97 mA^2, 31.43 mA^2] when 91 taps are used in the DD LMS equalization.

Considering the measured optical power at the receiver (P_{UTC}), it is confirmed that using 91 taps a received optical range from 8 to 15.5 dBm ensures adequate transmission meeting the HD-FEC BER threshold for both same-core and different cores transmission. Transmission in the same core enables up to $P_{UTC} < 16$ dBm and $I_{ph}^2 < 37.8$ mA^2, compared with different cores transmission of $P_{UTC} < 15.5$ dBm and $I_{ph}^2 < 31.43$ mA^2 due to saturation effects when combining both λ_D and λ_{LO} at the UTC.
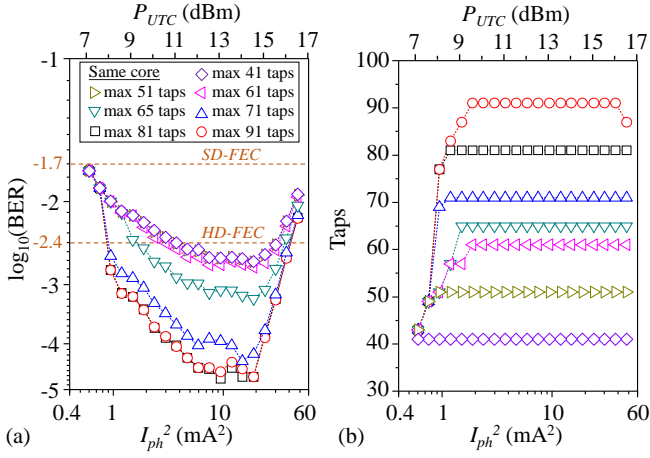
Fig. 6. Performance of optical transmission in the same core in 1-km MCF vs. received optical power (P_{UTC}) and squared photocurrent (I_{ph}^2): (a) measured BER and (b) number of taps employed for DD LMS equalization
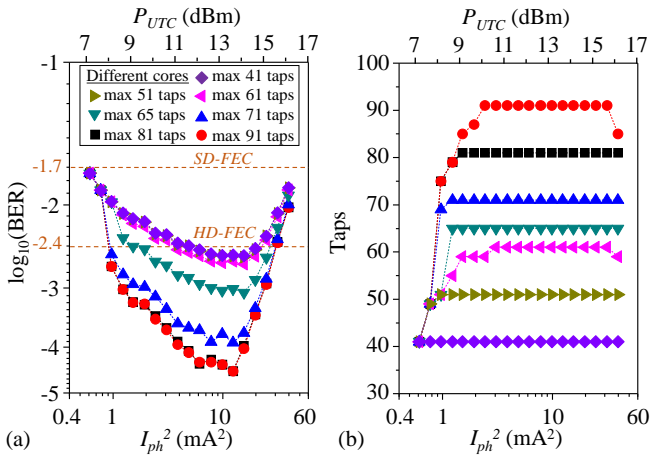

Fig. 7. Performance of optical transmission in different cores in 1-km MCF vs. received optical power (P_{UTC}) and squared photocurrent (I_{ph}^2): (a) measured BER and (b) number of taps employed for DD LMS equalization
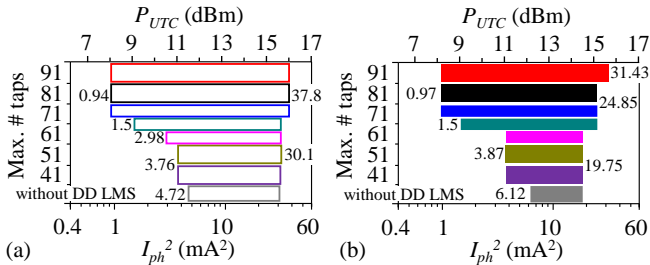

Fig. 8. Received optical power (P_{UTC}) and squared photocurrent (I_{ph}^2) range meeting the HD-FEC BER recommendation after 1-km MCF vs. maximum number of taps employed for DD LMS equalization when transmitted in: (a) the same core and (b) different cores, compared with no DD LMS

It can be observed in Fig. 6(b) and Fig. 7(b) that, for low received photocurrent levels ($I_{ph}^2 < 2$ mA^2), the number of taps used for DD LMS equalization is reduced, as increasing the order does not improve the BER due to the low signal to noise ratio (SNR).

Following the simulation study depicted in Section II.A, Fig. 9 shows the BER performance of a 16QAM 12.5 GBd signal evaluated with Optiwave for different optical signal to noise ratio (OSNR) levels after different fiber lengths. The simulation study confirms that the optical reach can be extended to 10 km and 25 km of fiber if the received OSNR > 10 dB for SD-FEC and > 13 dB for HD-FEC transmission.
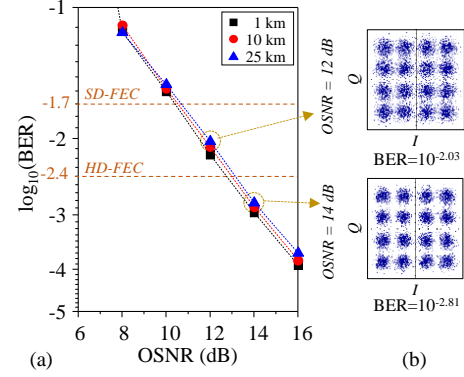

Fig. 9. (a) Simulated BER performance of a 16QAM 12.5 GBd signal over 1 km, 10 km and 25 km fiber transmission at λ_D=1552.62 nm and (b) example of received constellations for different OSNR
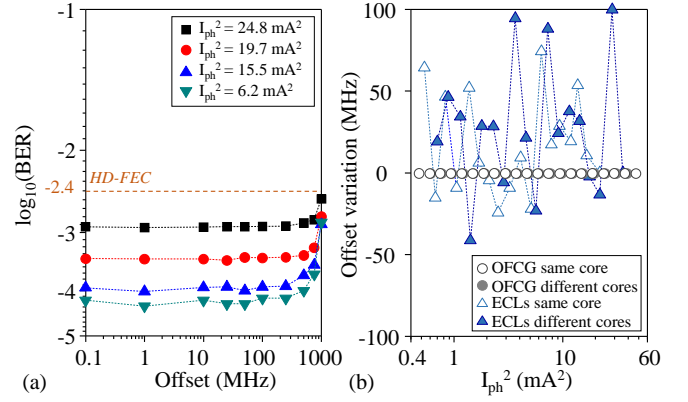

Fig. 10. (a) Measured BER performance of optical transmission in different cores in 1-km MCF processed with fixed 81 taps DD LMS with different frequency offset values from f_{up}=12.211984 GHz vs. offset. (b) Offset variation obtained with FOE and without DD LMS equalization over f_{up}=12.211984 GHz comparing OFCG and ECLs generation sent through the same core (c7) and through different cores (c4 and c7)

Next, we evaluate the performance of the system with the frequency offset. In this case, the DD LMS equalization is performed with a fixed number of taps of 81 (higher than 71 according to the previous result). The center frequency is set to f_{up}=12.211984 GHz (value that minimizes the offset in the FOE calculation to less than ±25 Hz) and then different frequency offsets are added from 0.1 MHz to 1 GHz. It can be observed in Fig. 10(a) that, for the same received photocurrent level, the BER performance remains almost constant for frequency offsets smaller than 100 MHz, suggesting that the DSP algorithms could be simplified for this application. Fig. 10(b) shows the obtained frequency offset variation when no DD LMS equalization is implemented, comparing with free-running lasers (ECLs) generation of the same λ_D and λ_{LO} being transmitted over both MCF systems described in Fig. 5.

It can be observed in Fig. 10(b) that using OFCG stabilizes the frequency offset variation in the kHz range, even when no DD LMS equalization is employed in the DSP, while using conventional generation with free-running ECLs presents a frequency offset variation of up to 74 MHz when the data and LO signals are transmitted over the same core and up to 100 MHz when transmitted over different cores.
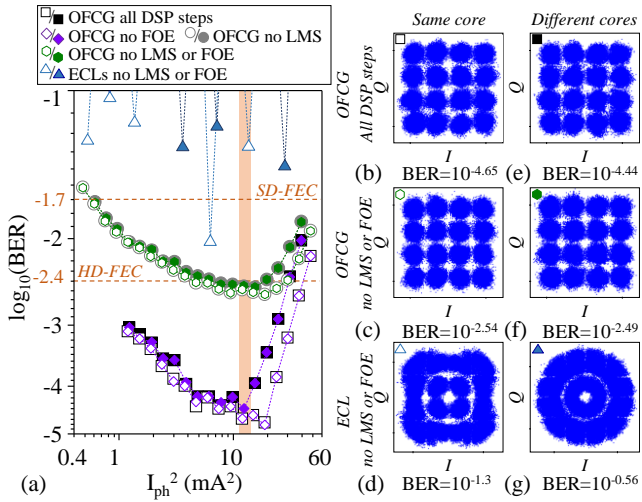
Fig. 11. (a) BER performance comparison vs. received squared photocurrent after 1-km 7-core MCF transmission (blank symbols for same core and filled symbols for different cores transmission). Received constellations marked with a shadow for transmission in the same core: (b) OFCG with all DSP steps for I_{ph}^2=12.01 mA^2, (c) OFCG without DD LMS or FOE for I_{ph}^2=12.01 mA^2; (d) ECL without DD LMS or FOE for I_{ph}^2=11.78 mA^2; and transmission in different cores: (e) OFCG with all DSP steps for I_{ph}^2=12.41 mA^2, (f) OFCG without DD LMS or FOE for I_{ph}^2=12.41 mA^2; and (g) ECL without DD LMS or FOE for I_{ph}^2=13.65 mA^2

The offset variation when ECL generation is used is slightly higher when transmitted over different cores due to the difference of the optical paths followed by the signals fed to a simplified DSP algorithm. The optical paths were not perfectly adjusted in the laboratory, as would happen in a real scenario. In this way, the DSP algorithm translates the different delays (optical phases) to different offsets. The optical setup is the same used with the optical comb evaluation, confirming the advantage of OFCG providing phase-noise correlated tones for both data and LO carriers. OFCG generation avoids the drawback of the phase noise resulting from the photonic mixing coming from the combination of the laser linewidths. This is evaluated further in Fig. 11 using simplified DSP algorithms (which remove the FOE or/and the DD LMS equalization steps) and comparing OFCG and ECL generation performance when transmitted over the same and different cores.

It is confirmed in Fig. 11(a) that, with OFCG wavelengths transmission in the same and different cores, the HD-FEC threshold recommendation is met when FOE and DD LMS equalization (with 81 taps) is implemented. Saturation at the photoreceiver is observed for photocurrent levels higher than 40 mA^2 when transmitted over the same core and than 30 mA^2 when transmitted over different cores. The photoreceiver saturation limits the available link budget to short wireless link configurations, adequate for high-performance rack-to-rack communications in datacenters, by example [11]. However, the link distance could be extended using of-the-shelf UTCs and different antenna configurations [22]. For example, using an antenna-integrated UTC [23] and 4×1 antenna array [24], a wireless distance of 5.9 m could be reached (or even 7 m if a 20%-overhead soft-decision SD-FEC is considered, i.e. BER 2×10^{-2} threshold). A 5 to 7 m wireless reach would be enough for indoor access in wireless local or personal access networks (WLAN or WPAN). However, longer distances could also be

reached using state-of-the-art THz amplification [25] and a Cassegrain antenna with 55 dBi gain [26], providing a coverage of up to 1200 m (or up to 1350 m considering SD-FEC) even in a heavy-rain scenario [22].

The BER performance for OFCG when no FOE nor DD LMS equalization is implemented is very similar when transmitting over the same core and over different cores with operating photocurrent range of [6 mA^2, 20 mA^2]. As an example, the received constellation for transmission over the same core is included in Fig. 11(c), compared with the similar constellation obtained for transmission over different cores included in Fig. 11(f). It can be observed in Fig. 11(a) that obtained BER when ECL generation is used without FOE nor DD LMS equalization does not meet the HD-FEC limit due to the instability of the frequency offset of the signal observed in Fig. 10(b), due to the phase difference of the data and LO carriers. The received constellations when ECL generation is used but no LMS or FOE is implemented confirm that the phase reference is lost in both cases, being more noticeable when transmitted over different cores –Fig. 11(g)– due to a higher frequency offset variation –Fig. 10(b)–. This confirms the suitability of using OFCG for the proposed application providing greater flexibility and simpler DSP thanks to the phase-correlated optical carriers.

IV. CONCLUSION

This paper demonstrates the suitability of a novel technique for remote photonic THz generation by using an OFCG and MCF media. We compared experimentally the performance of an optical backhaul system when transmitting the 16QAM 12.5 GBd data signal and LO for optical heterodyning over the same or over different cores in a 1-km MCF link. The experimental evaluation includes a short wireless link at 183 GHz center frequency over 13.75 GHz BW. Both implementations meet the HD-FEC BER recommendation for received optical power levels from 12 to 14.5 dBm, even when no DD LMS equalization is implemented in the DSP. This optical range can be extended using DD LMS. The experimental results confirm that using 91 taps in the DD LMS a received optical range from 8 to 15.5 dBm ensures HD-FEC transmission. The received optical range can be extended to 16 dBm when both data and LO wavelengths are transmitted in the same core. When the optical LO is transmitted in a different core, the optical power and photocurrent range is smaller, only reduced in the upper values due to saturation effects (with $I_{ph}^2 < 31.43$ mA^2 when 91 taps are used in the DD LMS for transmission in different cores, compared with $I_{ph}^2 < 37.8$ mA^2 in the same core).

Comb wavelength generation also permits simplifying the processing algorithms by removing FOE processing, as the BER performance remains almost constant for frequency offsets up to 100 MHz. OFCG generation also enables further simplification of the DSP processing by removing the DD LMS equalization, thanks to the phase correlation of the optical carriers. The experimental results confirm that this would not be possible with conventional ECL transmission due to the instability of the frequency offset of the received signals.

REFERENCES

[1] T. Schneider, A. Wiatrek, S. Preußler, M. Grigat, and R-P. Braun, "Link budget analysis for Terahertz fixed wireless links," *IEEE Trans. on Terahertz Science and Techn.*, vol. 2, no. 2, pp. 250-256, March 2012.

[2] A. J. Seeds, H. Shams, M. J. Fice, and C. C. Renaud, "TeraHertz photonics for wireless communications," *IEEE/OSA J. Lightw. Technol.*, vol. 33, no. 3, pp. 579-587, Feb. 2015.

[3] A. Nirmalathas, P. A. Gamage, C. Lim, D. Novak, and R. Waterhouse, "Digitized radio-over-fiber technologies for converged optical wireless access network," *IEEE/OSA J. Lightw. Technol.*, vol. 28, no. 16, pp. 2366-2375, Aug. 2010.

[4] H. Shams, T. Shao, M. J. Fice, P. M. Anandarajah, C. C. Renaud, F. Van Dijk, L. P. Barry and A. J. Seeds, "100 Gb/s multicarrier THz wireless transmission system with high frequency stability based on a gain-switched laser comb source," *IEEE Photonics Journal*, vol. 7, no. 3, 7902011, June 2015.

[5] H. Ito, S. Kodama, Y. Muramoto, T. Furuta, T. Nagatsuma, and T. Ishibashi,"High-speed and high-output InP-InGaAs unitraveling-carrier photodiodes," *IEEE J. Sel. Top. Quantum Electron*., vol. 10, no. 4, pp. 709-727, July-Aug. 2004.

[6] H. Zhang, M. Xu, J. Zhang, Z. Jia, L. A. Campos and C. Knittle, "Highly efficient full-duplex coherent optical system enabled by combined use of optical injection locking and frequency comb," *IEEE/OSA J. Lightw. Technol.*, vol. 39, no. 5, pp. 1271-1277, March 2021.

[7] S. J. Savory, "Digital coherent optical receivers: algorithms and subsystems," *IEEE J. Selected Topics in Quantum Electronics*, vol. 16, no. 5, pp. 1164-1179, Sept.-Oct. 2010.

[8] M. Morant, A. Macho and R. Llorente, "On the suitability of multicore fiber for LTE-Advanced MIMO optical fronthaul systems," *IEEE/OSA J. Lightw. Technol.*, vol. 34, no. 2, pp. 676-682, Jan. 2016.

[9] R. Rumipamba-Zambrano, J. Perelló and S. Spadaro, "Route, modulation format, MIMO, and spectrum assignment in flex-grid/MCF transparent optical core networks," *IEEE/OSA J. Lightw. Technol.*, vol. 36, no. 16, pp. 3534-3546, Aug. 2018.

[10] L. G. Guerrero, M. Morant, T. Li, M. J. Fice, A. J. Seeds, R. Llorente, I. H. White, R. V. Penty and C. C. Renaud, "Integrated wireless-optical backhaul and fronthaul provision through multicore Fiber," *IEEE Access*, vol. 8, pp. 146915-146922, Aug. 2020.

[11] C-L. Cheng and A. Zaji, "Characterization of 300 GHz wireless channels for rack-to-rack communications in data centers," in *Proc. 2018 IEEE 29th Annual International Symposium on Personal, Indoor and Mobile Radio Communications (PIMRC)*, pp. 194-198, Sept. 2018.

[12] G. K. M. Hasanuzzaman, H. Shams, C. C. Renaud, J. Mitchell, A.J. Seeds, S. Iezekiel, "Tunable THz signal generation and radio-over-fiber link based on an optoelectronic oscillator-driven optical frequency comb," *IEEE/OSA J. Lightw. Technol.*, vol. 38, no. 19, pp. 5240-5247, Oct. 2020.

[13] T. Sakamoto, T. Kawanishi and M. Izutsu, "Widely wavelength-tunable ultra-flat frequency comb generation using conventional dual-drive Mach-Zehnder modulator," *Electronics Letters*, vol. 43, no. 19, pp. 1-2, Sept. 2007.

[14] T. Sakamoto, T. Kawanishi and M. Izutsu, "Asymptotic formalism for ultraflat optical frequency comb generation using a Mach–Zehnder modulator," *OSA Opt. Letters*, vol. 32, no. 11, pp. 1515-1517, June 2007.

[15] X. Lin, M. Natrella, J. Seddon, C. Graham, C. C. Renaud, M. Tang, J. Wu, H. Liu, and A. J. Seeds, "High performance waveguide uni-travelling carrier photodiode grown by solid source molecular beam epitaxy," *OSA Opt. Exp.*, vol. 27, no. 25, pp. 37065-37086, Dec. 2019.

[16] I. Fatadin, D. Ives and S. J. Savory, "Blind equalization and carrier phase recovery in a 16-QAM optical coherent system," *IEEE/OSA J. of Lightwave Techn.*, vol. 27, no. 15, pp. 3042-3049, Aug. 2009.

[17] M. Selmi, C. Gosset, M. Noelle, P. Ciblat and Y. Jaouen, "Block-wise digital signal processing for polmux QAM/PSK optical coherent systems," *IEEE/OSA J. of Lightwave Techn.*, vol. 29, no. 20, pp. 3070-3082, Oct. 2011.

[18] M. Morsy-Osman, Q. Zhuge, L. R. Chen, and D. V. Plant, "Feedforward carrier recovery via pilot-aided transmission for single-carrier systems with arbitrary M-QAM constellations," *OSA Opt. Express*, vol. 19, no. 24, pp. 24331-24343, Nov. 2011.

[19] ITU-T Recom. Std. G.975.1, Forward error correction for high bit-rate DWDM submarine systems, 2004.

[20] X. Lin, M. Natrella, J. Seddon, C. Graham, C. C. Renaud, M. Tang, J. Wu, H. Liu, and A. J. Seeds, "High performance waveguide uni-travelling carrier photodiode grown by solid source molecular beam epitaxy," *OSA Opt. Express*, vol. 27, no. 25, pp. 37065-37086, Dec. 2019.

[21] C-L. Cheng, S. Sangodoyin and A. Zajić, "Terahertz MIMO fading analysis and doppler modeling in a data center environment," in *Proc. 14th European Conference on Antennas and Propagation (EuCAP)*, pp. 1-5, Mar. 2020.

[22] L. Gonzalez-Guerrero, H. Shams, I. Fatadin, J. E. Wu, M. J. Fice, M. Naftaly, A. J. Seeds and C. C. Renaud, "Pilot-tone assisted 16-QAM photonic wireless bridge operating at 250 GHz," *IEEE/OSA J. Lightw. Technol.,* vol. 39, no. 9, pp. 2725-2736, May 2021.

[23] E. Rouvalis, C. C. Renaud, D. G. Moodie, M. J. Robertson, and A. J. Seeds, "Continuous wave Terahertz generation from ultra-fast InP-based photo-diodes," *IEEE Trans. Microw. Theory Techn.*, vol. 60, no. 3, pp. 509-517, Mar. 2012.

[24] G. Sakano, J. Haruki, K. Sakuma, and K. Kato, "4-channel synchronous Thz-wave generator composed of arrayed UTC-PDs and antennas," in *Proc. 21st Optoelectron. Commun. Conf.*, pp. 1-3, July 2016.

[25] Z. Griffith, M. Urteaga, and P. Rowell, "180-265 GHz, 17-24 dBm output power broadband, high-gain power amplifiers in InP HBT," in *Proc. IEEEMTT-S Int. Microw. Symp.*, pp. 973-976, 2017.

[26] I. Kallfass, F. Boes, T. Messinger, J. Antes, A. Inam, U. Lewark, A. Tessmann and R. Henneberger, "64 Gbit/s transmission over 850 m fixed wireless link at 240 GHz carrier frequency," *Springer Journal of Infrared, Millimeter, and Terahertz Waves*, vol. 36, pp. 221-233, 2015.